NTNU

Kunnskap for en bedre verden

Department of Mathematical Sciences

TMA4112 - Numerical solution of differential equations by difference methods

Project 1

Authors:
Hanna Rød, Thea Boge, Karine Grande

28.02.2025

Table of Contents

1 Introduction

Reaction-diffusion equations are widely used to model physical, chemical, and biological processes, where diffusion and reaction dynamics interact over time. In this project, we analyze numerical methods for solving such equations, focusing on a modified Crank-Nicolson scheme that combines implicit and explicit approaches for efficiency and accuracy. We begin with a theoretical analysis of the method's consistency and stability, followed by numerical experiments to validate these results. Through this work, we aim to assess the method's effectiveness.

Moreover, we will look at a spatially extended SIR epidemic model to study the spread of infectious diseases. This involves solving a reaction-diffusion equation, and hence simulating the spread of infection in space and time. From here we will explore different scenarios for our model.

2 Theoretical Analysis of the Numerical Method

In this section, we analyze the consistency, stability, and global error of the proposed numerical scheme for the reaction-diffusion equation given by

$$u_t = \mu u_{xx} + f(u), \tag{1}$$

where μ is the diffusion coefficient and $f(u) = au$, where a is a constant, represents the linear reaction term. The modified Crank-Nicolson scheme is given by

$$U_m^* = U_m^n + \frac{r}{2}(\delta_x^2 U_m^* + \delta_x^2 U_m^n) + kf(U_m^n), \tag{2}$$

$$U_m^{n+1} = U_m^* + \frac{k}{2}(f(U_m^*) - f(U_m^n)), \tag{3}$$

where $r = \frac{\mu k}{h^2}$. Here k and h are the step sizes in time and space respectively.

We establish the consistency, Von Neumann stability, and the global error of the scheme by proving the following theorems.

2.1 Theorem 1 - Consistency of the Scheme

The modified Crank-Nicolson scheme given by (2) and (3) is consistent with the reaction-diffusion equation (1) with a local truncation error of order $\tau_m^n = O(k^2 + h^2)$.

Proof. To establish consistency, we substitute the exact solution $u_m^n = u(x_m, t_n)$ into the numerical scheme and expand in a Taylor series.

First, solving for U_m^* from (2), we obtain:

$$U_m^* = \frac{U_m^{n+1} + \frac{ak}{2}U_m^n}{1 + \frac{ak}{2}}.$$

Substituting into (3) gives:

$$\frac{U_m^{n+1} + \frac{ka}{2}U_m^n}{1 + \frac{ka}{2}} = (1 + ka)U_m^n + \frac{r}{2}\left[\frac{\delta_x^2 U_m^{n+1}}{1 + \frac{ka}{2}} + \frac{(1 + ka)\delta_x^2 U_m^n}{1 + \frac{ka}{2}}\right],$$

which expands to:

$$\begin{aligned} U_m^{n+1} = (1 + ka + \frac{(ka)^2}{2})U_m^n \\ + \frac{r}{2}\Big[U_{m+1}^{n+1} - 2U_m^{n+1} + U_{m-1}^{n+1} + (1 + ka)(U_{m+1}^n - 2U_m^n + U_{m-1}^n)\Big]. \end{aligned}$$

Rearranging and simplifying:

$$U_m^{n+1}(1+r) = U_m^n(1+ka+\frac{(ka)^2}{2}-r-kar) + \frac{r}{2}U_{m+1}^{n+1}+\frac{r}{2}U_{m-1}^{n+1}+\frac{r}{2}(1+ka)U_{m+1}^n+\frac{r}{2}(1+ka)U_{m-1}^n.$$

Using a Taylor expansion around (x_m, t_n), and neglecting higher-order terms, we obtain:

$$u_t+\frac{1}{2}ku_{tt}+\frac{1}{6}k^2u_{ttt} = au+\frac{ak^2}{2}u+\mu u_{xx}+\frac{h^2}{12}\mu u_{xxxx}+\frac{k}{2}\mu u_{xxt}+\frac{k}{2}a\mu u_{xx}+\frac{kh^2}{12}a\mu u_{xxxx}.$$

From the PDE (1), we substitute:

$$\mu u_{xx} = u_t - au \qquad\qquad \mu u_{xxt} = u_{tt} - au_t.$$

Thus, the local truncation error is given by:

$$|\tau_m^n| \le \frac{1}{6}k^2|u_{ttt}| + \frac{h^2}{12}\mu|u_{xxxx}| + \frac{h^2k\mu}{2}|u_{xxxx}| = O(k^2+h^2+h^2k) = O(k^2+h^2).$$

This proves the scheme is consistent for the reaction-diffusion equation with local truncation error $\tau_m^n = O(k^2+h^2)$. □

2.2 Theorem 2 - Stability of the Scheme

The modified Crank-Nicolson scheme satisfies the Von Neumann stability criterion, and is therefore unconditionally stable. This means there exists a constant $\mu \ge 0$ such that

$$|\xi| \le 1 + k\mu,$$

where $|\xi|$ is the amplification factor.

Proof. Using a Fourier mode solution, we assume

$$U_m^n = \xi^n e^{i\beta x_m},$$

where ξ is the amplification factor, β is the wave number, and $x_m = mh$ represents the spatial discretization points. Our goal is to express U_m^{n+1} in terms of U_m^n, then use this result to find a bound for $|\xi|$.

Start by rewriting (2). Using the Fourier mode solution, we obtain the following expression for $\delta_x^2 U_m^n$

$$\begin{aligned}\delta_x^2 U_m^n &= U_{m+1}^n - 2U_m^n + U_{m-1}^n \\ &= \xi^n e^{i\beta(x_m+h)} - 2\xi^n e^{i\beta x_m} + \xi^n e^{i\beta(x_m-h)} \\ &= \xi^n e^{i\beta x_m}\left(e^{i\beta h} - 2 + e^{-i\beta h}\right) \\ &= U_m^n(2(\cos\beta h - 1)) \\ &= 2\sigma U_m^n,\end{aligned}$$

Thus, (2) can be expressed as

$$U_m^* = \frac{(1+ka+r\sigma)}{(1-r\sigma)}U_m^n,$$

where $\sigma = \cos \beta h - 1$.

Substituting this into (3), we obtain:

$$\begin{aligned} U_m^{n+1} &= \left(\frac{1 + ka + r\sigma + kar\sigma}{1 - r\sigma} + \frac{\frac{k^2 a^2}{2}}{1 - r\sigma} \right) U_m^n \\ &\leq \left((1 + ka) \frac{1 + r\sigma}{1 - r\sigma} + \frac{k^2 a^2}{2} \right) U_m^n, \end{aligned}$$

since $1 - r\sigma \geq 1$. Furthermore, since $\sigma \leq 0$, it follows that:

$$\frac{1 + r\sigma}{1 - r\sigma} \leq 1 \quad \text{for all } \beta.$$

Thus, we conclude:

$$U_m^{n+1} \leq \left(1 + k \left(a + \frac{ka^2}{2} \right) \right) U_m^n.$$

Applying the Fourier mode solution again, we substitute $U_m^n = \xi^n e^{i\beta x_m}$ and $U_m^{n+1} = \xi^{n+1} e^{i\beta x_m}$. Dividing by $\xi^n e^{i\beta x_m}$, we obtain:

$$|\xi| \leq 1 + k \left(a + \frac{Ta^2}{2} \right),$$

where T is the size of the domain Ω, i.e., the largest step size possible. The term $a + \frac{Ta^2}{2}$ is simply a constant $\mu \geq 0$. Finally, we get:

$$|\xi| \leq 1 + k\mu,$$

which proves that the modified Crank-Nicolson scheme is unconditionally stable. □

2.3 Global Error of the Scheme

The Von Neumann stability analysis assumes a periodic function in space. This allows us to analyze the growth of Fourier modes by substituting solutions of the form:

$$U_m^n = \xi^n e^{i\beta x_m}.$$

From the stability criterion, we ensure that the amplification factor ξ satisfies:

$$|\xi| \leq 1 + O(k),$$

which confirms that the error does not grow uncontrollably. However, Von Neumann analysis alone does not guarantee absolute stability since it does not account for boundary effects. To ensure stability in the general case, we assume periodic boundary conditions.

The Lax Equivalence Theorem (Owren 2017) states that: "A consistent difference scheme is convergent if and only if it is stable."

Since we have already shown consistency, proving absolute stability now ensures convergence. That is, as $h, k \to 0$, the numerical solution U_m^n converges to the true solution $u(x_m, t_n)$.

For a convergent scheme, the global error is typically of the same order as the local truncation error. This happens because the global error is the accumulation of local truncation errors over time. Since the scheme is stable, these errors do not grow uncontrollably. Consequently, we expect the global error to satisfy

$$\|E^n\| = O(k^2 + h^2).$$

In the following numerical experiments, we will further examine this behavior.

2.4 Numerical experiments

To validate our theoretical results, we implement the numerical scheme in Python. To optimize our reaction-diffusion solver, we utilize SciPy's LAPACK interface.

We use the test case:

$$u_t = \mu u_{xx} + au \tag{4}$$

with Dirichlet boundary conditions, and initial condition:

$$u(x, 0) = \sin\left(\frac{\pi x}{L}\right) \tag{5}$$

The exact solution is given by:

$$u(x, t) = e^{\left(a - \mu \frac{\pi^2}{L^2}\right)t} \sin\left(\frac{\pi x}{L}\right) \tag{6}$$

We begin by solving our test case with the numerical scheme and comparing the solution to the analytical solution at the last time step. This is plotted in Figure 1.

As expected, the global error is observed to decrease with decreasing h and k values, as shown in Figure 2 and Figure 3. Our convergence plots both have a slope of 2, confirming the method being of order 2 in both space and time.

3 Application

Now we will look at an epidemiological model that evolves in space and time. A widely used mathematical model to describe the spread of infectious diseases is the SIR model, governed by the following system of ordinary differential equations:

$$\begin{aligned} \frac{dS}{dt} &= -\beta SI, \\ \frac{dI}{dt} &= \beta SI - \gamma I, \\ \frac{dR}{dt} &= \gamma I. \end{aligned} \tag{7}$$

Here, β represents the transmission rate, and γ is the removal rate. We assume a scaled model, where S - Susceptible, I - Infected, and R - Removed, represent the fractions of the total population in each compartment, satisfying:

$$S(t) + I(t) + R(t) = 1.$$

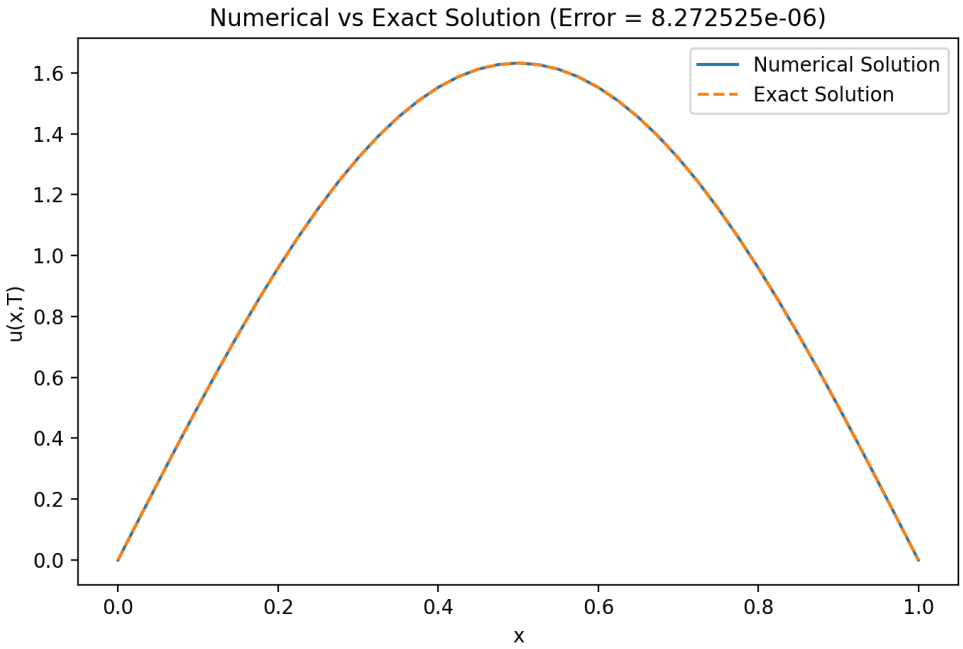

Figure 1: Numerical vs. exact solution of test equation at last time step.

To incorporate spatial spread, diffusion terms are added to the model, leading to the following system of partial differential equations (Murray 2003):

$$\begin{aligned} S_t &= -\beta IS + \mu_S \Delta S, \\ I_t &= \beta IS - \gamma I + \mu_I \Delta I. \end{aligned} \tag{8}$$

where μ_S and μ_I are diffusion coefficients that model the rate at which individuals move through space, and the Laplacian operator Δu is defined as

$$\Delta u = u_{xx} + u_{yy}.$$

As a start, we assume a small portion of the population is infected in the middle of our grid at time $t = 0$, and see how the disease will spread from there. For now, we choose $\beta = 3.0$, $\gamma = 1.0$, $\mu_S = 0.01$ and $\mu_I = 0.02$. The spread for this case is visualized as a Matplotlib animation in application.py and an excerpt of it is given in Figure 4. The plots show a circular spread, where after a while, we get a torus shape. This tells us that the population in the center are, given some time, removed individuals.

Changing to a higher β-value will give us larger transmission of the infection. A larger transmission rate can example-wise indicate few infection control measures. A plot for $\beta = 6.0$ is shown in Figure 5. Here we can see the infection spreading at a faster rate than previously.

For the next demonstration, we set β back to 3.0, and choose $\gamma = \beta$, meaning a higher removal rate than what we used for the base case. A high removal rate can be chosen to model an infection that either heals rapidly or is highly deadly. From Figure 6 we observe that the infection is spreading by a very small amount. Hence, choosing an even larger γ-value will evidently, if high enough, stop the infection from spreading.

Now we look at a case with $\mu_S = 0.005$ and $\mu_I = 0.1$, meaning we should see a rapid spread of infection in our model. Exactly this is shown in Figure 7. This type of model can for example be used for groups of people that tend to move around fast, perhaps for a young group of people.

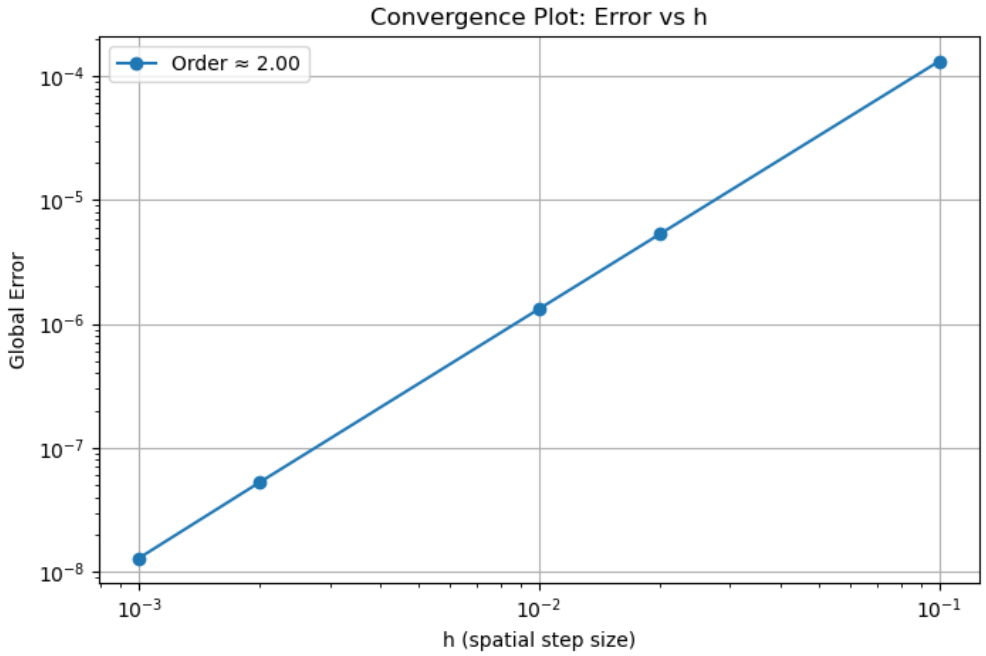

Figure 2: Convergence plot showing global error against spatial step size h. The method is order 2 accurate in space.

Furthermore, we go back to our base case and look at some more intricate examples. Figure 8 shows the spread over time when initializing the population as infected at three points on the grid in a diagonal. This makes for interesting plots when the separated regions meet.

Lastly, we have implemented a model with a moving superspreader. We do this by using a dynamically shifting infection source that follows a circular trajectory within the spatial domain. This approach can model scenarios where, as an example, some infectious individuals travel a circular route through a population, and hence continuously introduce new infection points.

4 Conclusion

The modified Crank-Nicolson scheme proves to be both unconditionally stable and accurate for solving reaction-diffusion equations. Numerical experiments confirm its consistency and second-order accuracy both in time and space, aligning with theoretical predictions. These results underscore the scheme's effectiveness as a reliable and efficient approach for handling diffusion-reaction dynamics.

In addition, we applied a numerical approach to solve a spatially extended SIR epidemic model. By varying parameters and introducing mobility effects, such as a moving superspreader, we explored different outbreak scenarios. The results highlight the impact of spatial diffusion on infection transmission and demonstrate the usefulness of numerical simulations.

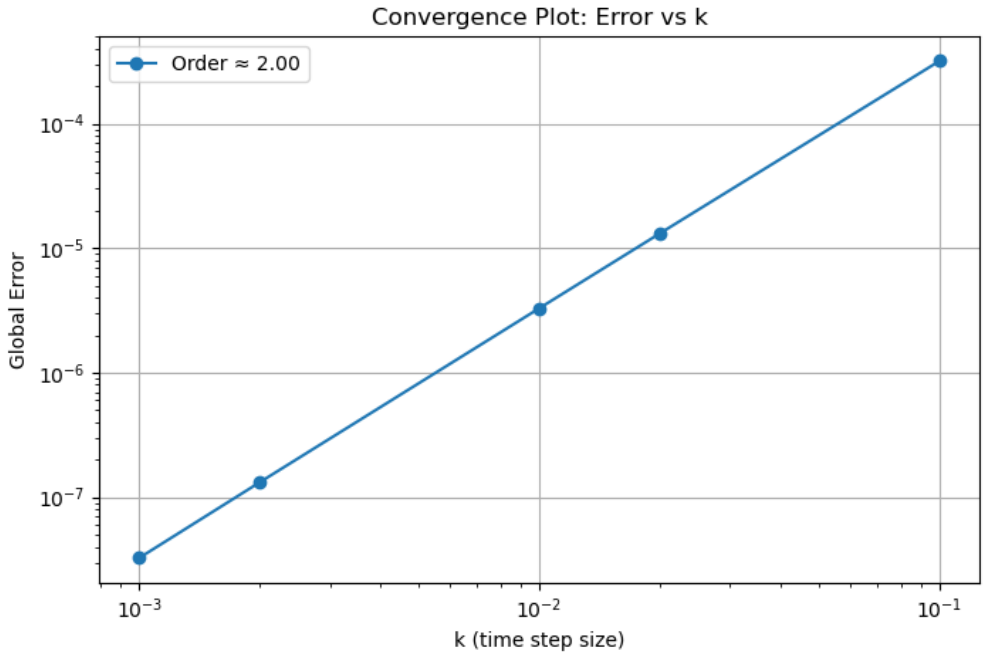

Figure 3: Convergence plot showing global error against time step size k. The method is order 2 accurate in time.

Bibliography

Murray, J.D. (2003). *Mathematical Biology II: Spatial Models and Biomedical Applications*. 3rd. Springer.

Owren, Brynjulf (2017). *TMA4212 Numerical solution of partial differential equations with finite difference methods*. Tech. rep. Lecture notes. Norwegian University of Science and Technology (NTNU).

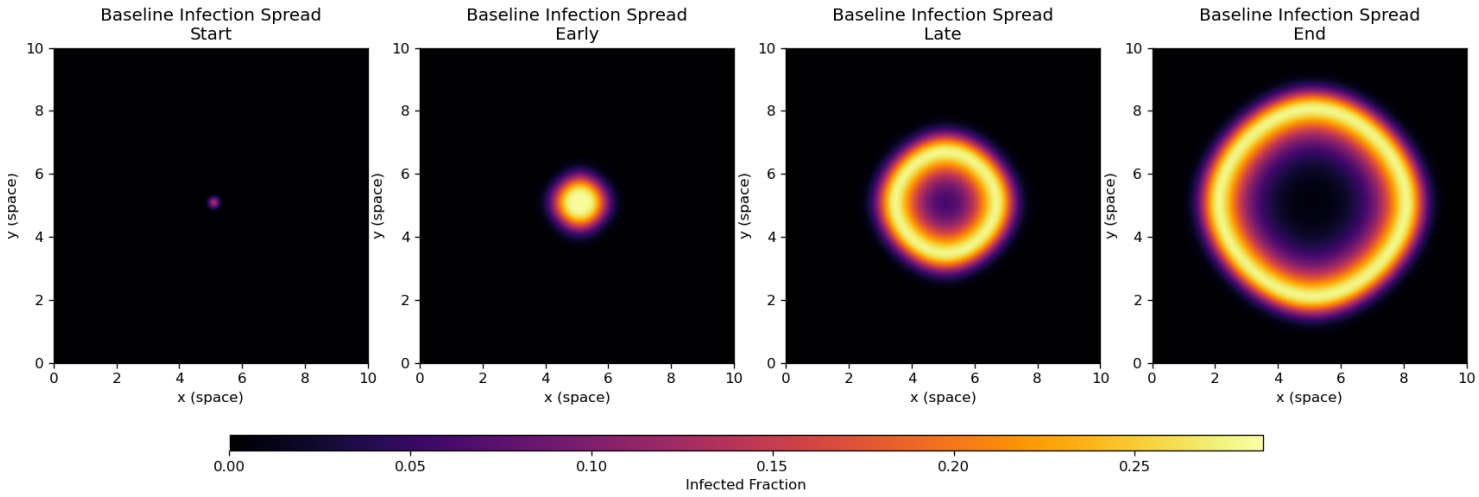

Figure 4: Infection spread over time when starting with a small portion of the population as infected in the middle of our grid. Here $\beta = 3.0$ and $\gamma = 1.0$.

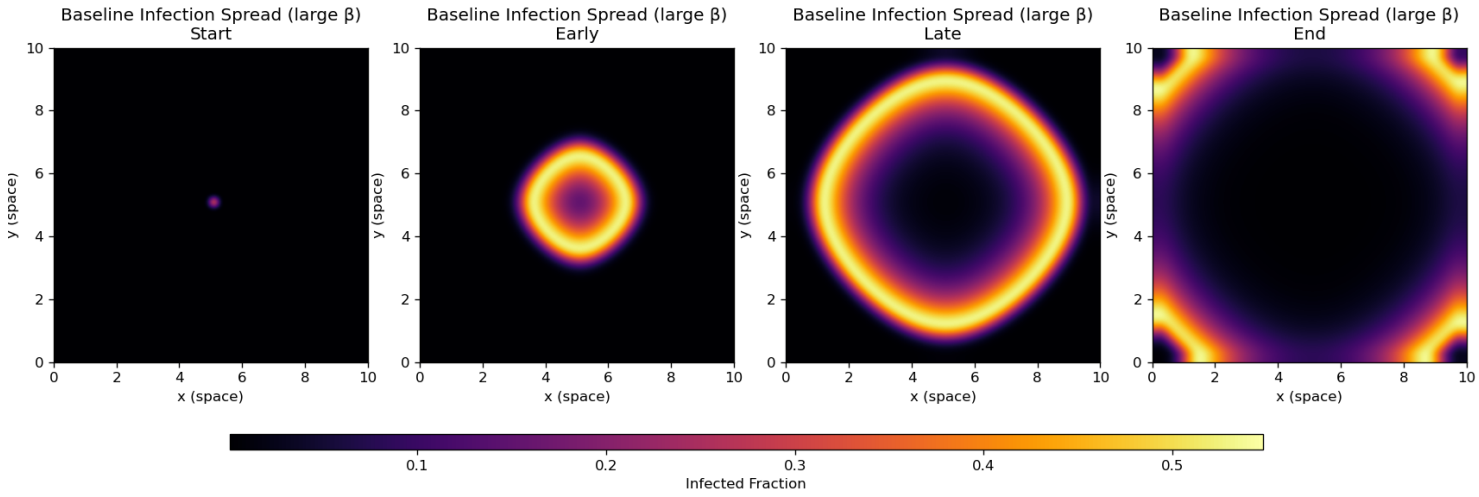

Figure 5: Infection spread over time when starting with a small portion of the population as infected in the middle of our grid, but with a larger transmission rate. Here $\beta = 6.0$ and $\gamma = 1.0$.

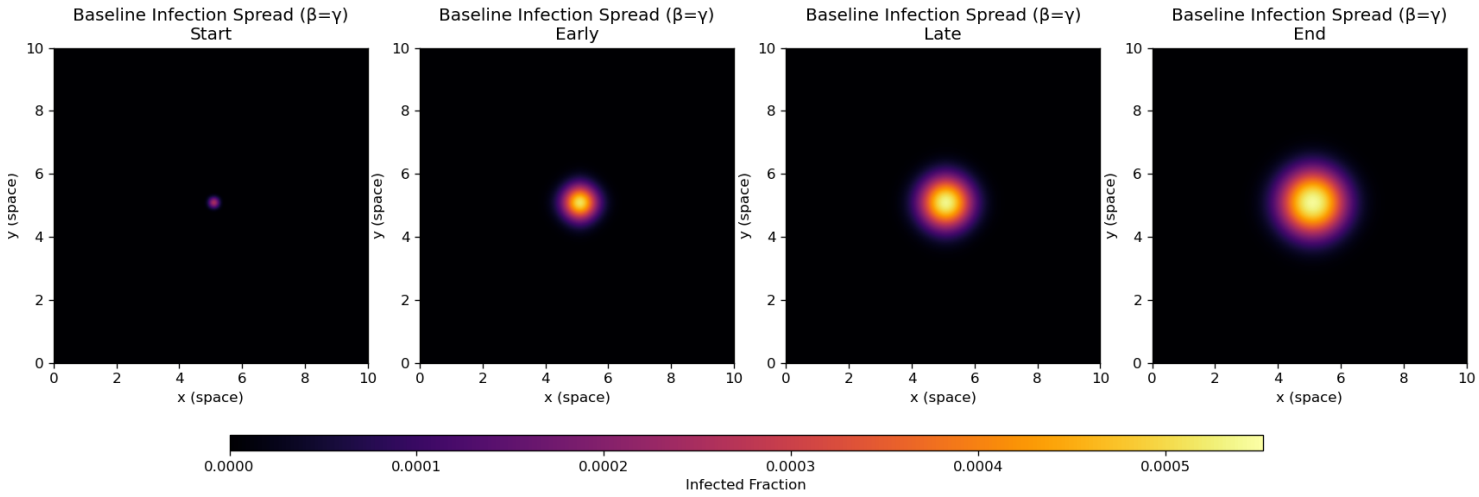

Figure 6: Infection spread over time when starting with a small portion of the population as infected in the middle of our grid, but with $\beta = \gamma = 3.0$.

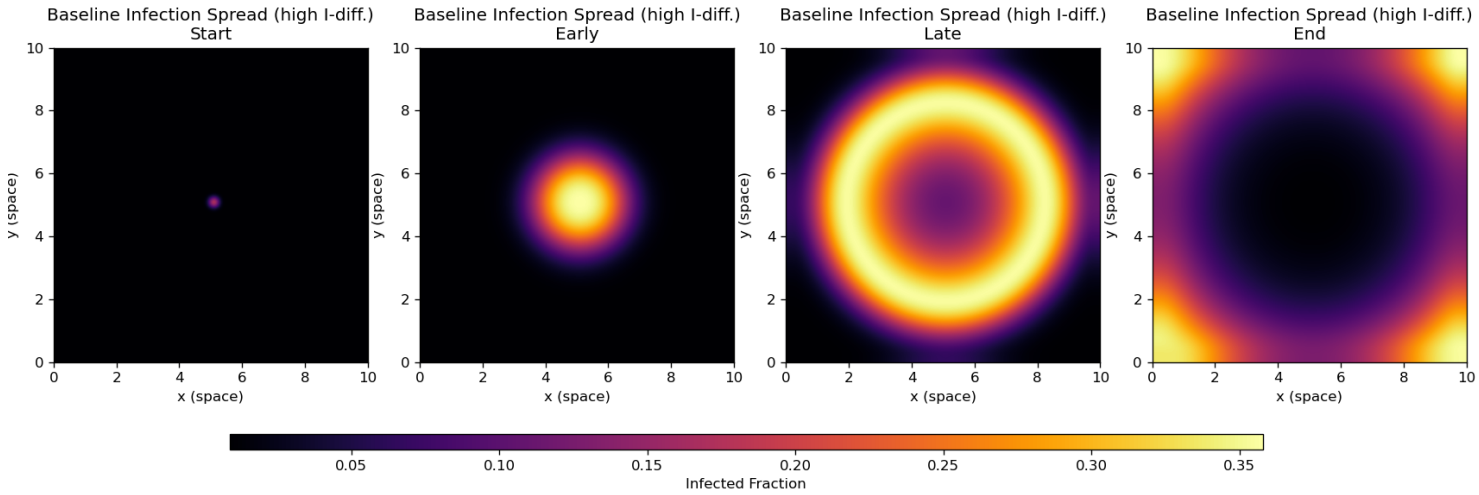

Figure 7: Infection evolving over time for $\mu_S = 0.005$ and $\mu_I = 0.1$, meaning μ_I is high. Here $\beta = 3.0$ and $\gamma = 1.0$.

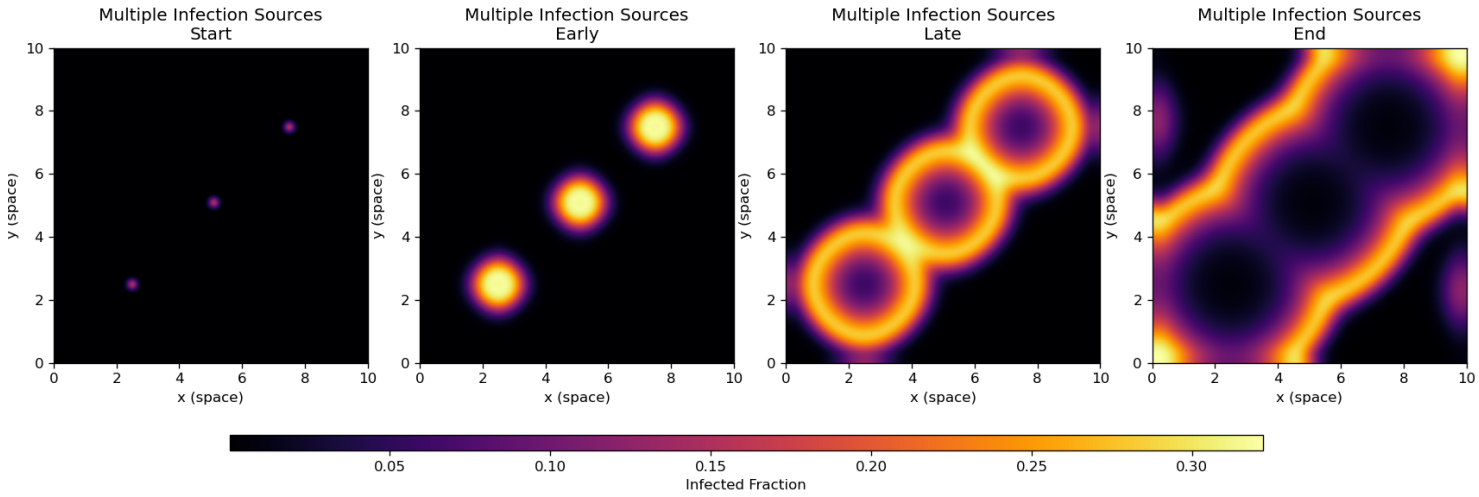

Figure 8: Infection spread over time when starting with small portions of the population as infected at three separate locations on our grid. Here $\beta = 3.0$ and $\gamma = 1.0$.

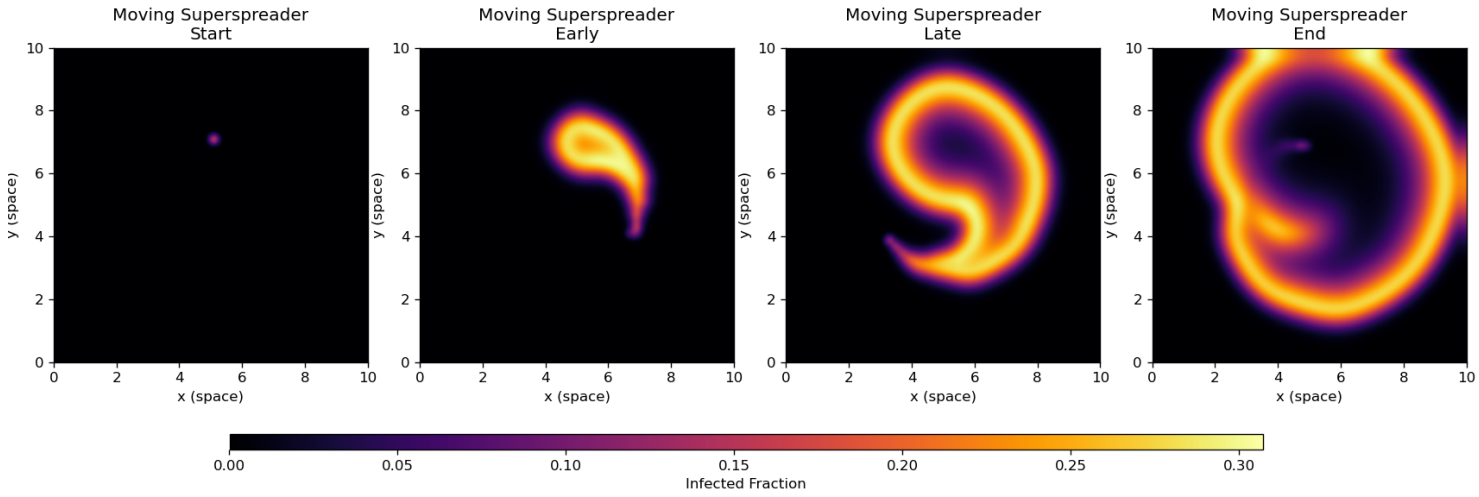

Figure 9: Infection spread over time when letting a superspreader move in a circular trajectory. Here $\beta = 3.0$ and $\gamma = 1.0$.